9-2020

Deformation and toughness behavior of β -type titanium alloys comprising C15-type Laves phase

C. D. Rabadia
Edith Cowan University

Y. J. Liu

S. F. Jawed
Edith Cowan University

L. Q. Wang

H. Sun
Edith Cowan University

See next page for additional authors

10.1016/j.mtsust.2020.100034

Deformation and toughness behavior of beta-type titanium alloys comprising C15 type Laves phase

C.D. Rabadia[a, *], Y.J. Liu[b], S.F. Jawed[a], L.Q. Wang[c,**], H. Sun[a], L.C. Zhang[a,*]

[a] *School of Engineering, Edith Cowan University, 270 Joondalup Drive, Joondalup, Perth, WA 6027, Australia*

[b] *School of Engineering, The University of Western Australia, 35 Stirling Highway, Perth, WA 6009, Australia*

[c] *State Key Laboratory of Metal Matrix Composites, School of Material Science and Engineering, Shanghai Jiao Tong University, No. 800 Dongchuan Road, Shanghai 200240, China*

Abstract

Laves phases are effective in tailoring the mechanical properties of alloys used for structural engineering applications. Therefore, it is an emerging research significance to investigate the deformation features of alloys comprising a Laves phase. In this work, the Ti-33Zr-xFe-yCr (x = 5, 7 wt% and y = 2, 4 wt%) alloys were designed in such a way that a Laves phase would form in the investigated Ti-33Zr-xFe-yCr alloys and later, cast by cold crucible levitation melting. All the as-cast alloys exhibit a face-centered cubic C15-type Laves phase along with a dominant β phase. The volume fraction of C15-Laves phase increases as the quantities of Fe and Cr increase in the Ti-33Zr-xFe-yCr alloys. Further, the volume fraction of C15-Laves phase influences the size of the deformation zone around the indentations and hardness of the investigated Ti-33Zr-xFe-yCr alloys. Vickers microindentation technique was used at the three different loads to examine the deformation features (around the indentations) of the as-cast alloys. In this work, Ti–33Zr–5Fe–2Cr shows large plastic strain (37.0%) in compression testing and high (true) yield strength (1,083 MPa) and hardness (3.50 GPa), whereas Ti-33Zr-

*Corresponding author. Email addresses: crabadia@our.ecu.edu.au; chiragrabadia@gmail.com (C.D. Rabadia)
*Corresponding author. Email address: l.zhang@ecu.edu.au; lczhangimr@gmail.com (L.C. Zhang)
** Co-corresponding author. Email address: wang_liqiang@sjtu.edu.cn (L.Q. Wang)

7Fe-4Cr demonstrates the highest (true) yield strength (1285 MPa), hardness (4.08 GPa), and the lowest size of the deformation zone around the indentations at three different indentation-loads. Moreover, the indentation-based fracture toughness of Ti-33Zr-7Fe-2Cr and Ti-33Zr-7Fe-4Cr were estimated based on the various relevant models proposed in the established literature.

Keywords: Laves phase; Deformation; Fracture toughness; Mechanical properties; Indentation; Titanium alloys.

1. Introduction

Alloys comprising AB_2-type Laves phases have become promising materials for high-strength structural applications in aerospace, automobile, nuclear and petrochemical industries because Laves phases produce superior strengthening effects in metallic alloys [1]. The three different variants of Laves phases are available: a hexagonal close-packed (hcp) C14 (with $MgZn_2$ type prototype structure), a face-centered cubic (fcc) C15 (with $MgCu_2$ type prototype structure), and a dihexagonal C36 (with $MgNi_2$ type prototype structure) [2, 3]. C14, C15, and C36 are the fundamental categories of Laves phases in which various phases with AB_2 compositions (with different alloying elements) form. In AB_2 alloy compositions, atoms of A comprise relatively larger atomic size (e.g., La, Ce, Zr, and B), whereas atoms of B comprise relatively smaller atomic size (e.g., Fe, Co, Mn, Ni, and Cr) [3, 4]. Laves phases in alloys mainly precipitate based on the values of atomic radii ratio (R_A/R_B), average valence electron concentration, and difference in electronegativities of A and B atoms present in AB_2 alloy compositions [5]. Fracture toughness is one of the important properties for the alloys used in high-strength structural applications. The fracture toughness values of alloys comprising Laves phase have been reported from around 0.5 to 2.2 $MPa{\cdot}m^{1/2}$ in previous findings [6-9]. These values indicate brittle nature of Laves phases. Nonetheless, deformability and fracture toughness of Laves phases can be improved by alloying brittle Laves phases with a soft

microstructure matrix possessing a large deformability [10, 11]. The β phase of Ti (with body-centered cubic (bcc) crystal structure) is quite popular to show large deformability [12-15]. Therefore, if Laves phases precipitate in the β matrix of Ti alloys, Laves phases would serve as a strengthening agent and β matrix would help to increase bulk deformability of an alloy [9]. As far as alloying elements of Ti alloys are concerned, Zr has a good affinity with Ti because both elements reside in a same group of the periodic table of elements. In addition, Zr also helps to improve mechanical and corrosion properties of Ti alloys [1, 16]. On the other hand, Fe and Cr are inexpensive solute elements, which increase yield strength and hardness of Ti alloys [17-20]. Hence, considering the aforementioned points, four titanium based alloys, Ti-33Zr-5Fe-2Cr (TZ52), Ti-33Zr-5Fe-4Cr (TZ54), Ti-33Zr-7Fe-2Cr (TZ72) and Ti-33Zr-7Fe-4Cr (TZ74), which demonstrate the C15 type Laves phase in the β matrix, have been chosen in the present work from our previous work [10]. Note that the quantities of alloying elements are in wt%.

Micro-indentation technique is effective in anlyzing deformation features of metallic materials [21]. The indentation-based deformation features correlate directly with the corresponding mechanical properties of materials [22]. Moreover, indentation methods are simple and less costly as compared to other mechanical testing methods [21]. Therefore, it is a great significance to analyze the combined elasto-plastic deformation behavior of a relatively hard C15 type Laves phase in the soft β matrix of titanium based Laves phase alloys.

The volume fraction of Laves phase significantly influence the mechanical properties of alloys [1, 23]. Therefore, the present work intends to investigate the true mechanical properties of the investigated Ti-33Zr-xFe-yCr alloys. Other than this, the present work aims to investigate the effects of volume fraction of C15 phase ($V_{f, C15}$) on the mechanical and indentation-based bulk deformation behavior of the investigated Ti-33Zr-xFe-yCr alloys because the investigated Ti-33Zr-xFe-yCr alloys comprise the different fraction of the C15 type Laves phase in the β

matrix. Further, the Vickers indentation-based fracture toughness of TZ72 and TZ74 have been investigated using the various relevant models proposed in the established literature [24, 25].

2. Materials and methods

The Ti-33Zr-xFe-yCr (x = 5, 7 wt% and y = 2, 4 wt%) were cast (in the form of ingots) using a cold crucible levitation melting technique which is effective to cast alloys having elements with a significant difference in melting point temperatures. The investigated Ti-33Zr-xFe-yCr alloys were remelted and flipped at least 5 times to obtain the chemical homogeneity and then, rapid quenching was performed in a water-cooled copper crucible to solidify the cast ingots of each investigated alloy. The Ti-33Zr-xFe-yCr alloys are now onwards abbreviated as the TZFC alloys. The multiple cylindrical rods were cut from the core of the ingots using wire electrical discharge machining. The cylindrical rods of each investigated alloy were sectioned (as per the requirement of analyses used in the present work) using a Buehler Isomet High Speed Pro precision cutting machine.

For microstructure analyses and hardness testing, the samples of each investigated alloy were first ground using SiC papers (subsequently up to 4000 grits) and then, polished using a Struers MD-Chem cloth and by adding a Struers OP-S colloidal silica liquid on the polishing cloth. Scanning electron microscopy (SEM) was performed with a backscattered electron detector using a FEI Verios XHR 460 scanning electron microscope. The volume fraction of each phase present in the investigated alloys were estimated using a threshold function of ImageJ software. The mechanical compression tests were performed on at least three samples of each investigated alloy at a crosshead speed of 0.1 mm/min using an Instron 5982 universal mechanical testing machine. For the TZFC alloys, true compressive stress and true compressive strain were calculated using Eqs. (1) and (2) respectively [26].

$$\varepsilon_{True} = -ln(1-\varepsilon) \quad (1)$$

$$\sigma_{True} = \sigma_{Eng} \cdot (1-\varepsilon) \quad (2)$$

where ε_{True} is true strain, ε is engineering strain, σ_{True} is true stress, σ_{Eng} is engineering stress. Vickers micro-hardness testing was executed for each investigated alloy at three different loads: 3 kgf (HV3), 10 kgf (HV10) and 30 kgf (HV30) and a holding time of 20 s using a Zwick Roell ZHU hardness tester. At least eight micro-indents at all the three loads were taken for each investigated alloy and the average hardness values were considered. Optical microscopy was executed using a Zeiss Axiocam optical microscope to capture the morphologies of hardness indentations for each investigated alloy. ImageJ software was used to measure lamellar spacing, crack-length and the size of the deformation zones (around the indentations).

3. Results and discussion

Phase and microstructure analyses have already been carried out for the investigated TZFC alloys in our previous finding (Ref. [10]), which reveal the C15 type Laves (fcc structure from a space group: Fd-3m) and β phases (bcc structure from a space group: Im-3m) in the TZ52, TZ54, TZ72 and TZ74 alloys. Fig. 1 shows the microstructural morphologies of the as-cast TZFC alloys including the white precipitated C15 type Laves phase in the β matrix (dark grey). C15 type Laves phase precipitates in the investigated TZFC alloys because R_A/R_B ratio for the Ti-Zr-Fe-Cr system is greater than 1.200, which is very close to the ideal R_A/R_B value (1.225) for the precipitation of Laves phase in the investigated Ti-33Zr-xFe-yCr alloys [10, 27]. Consequently, C15 type Laves phase precipitates in the investigated alloys due to the atomic size misfit effect [3].

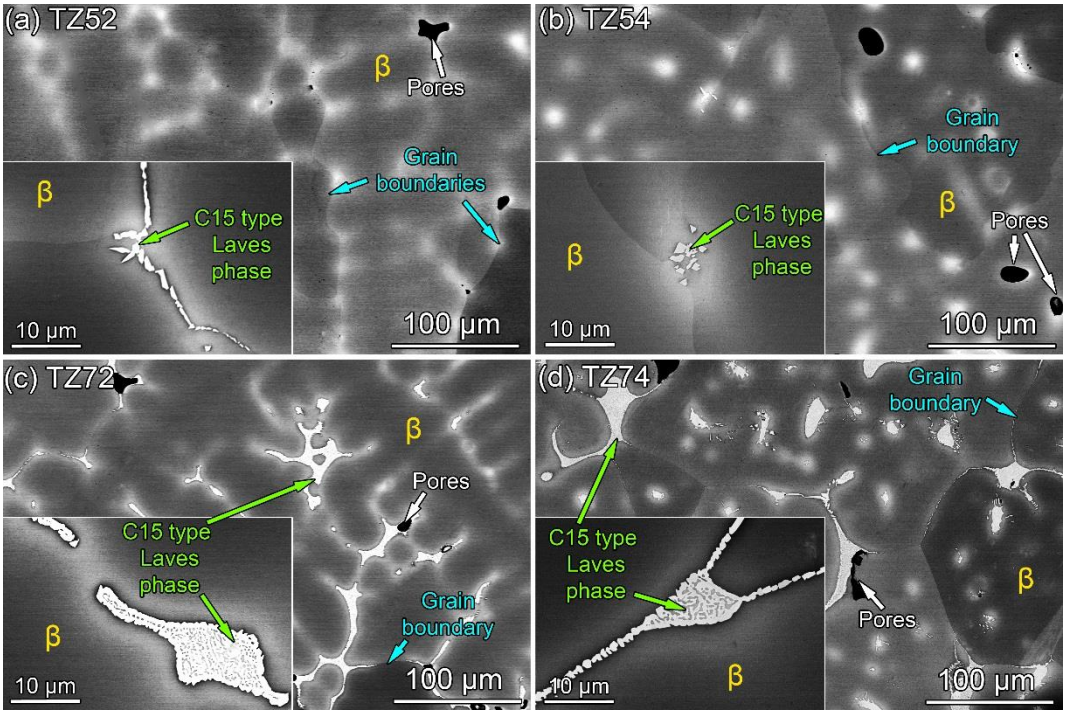

Fig. 1. The microstructural (backscattered SEM) morphologies of the investigated TZFC (Ti-33Zr-xFe-yCr) alloys which are labelled in the form of TZxy. The inset images show the magnified morphologies of C15 type Laves phase for each investigated alloy.

The formation of C15 type Laves phase in the TZFC alloys also reveal the solubility limit of Fe and Cr in Ti-33Zr alloys. This phenomenon should be considered while designing titanium-based alloys using eutectoid type β stabilizers, i.e., Fe and Cr for a specific application. Furthermore, the volume fraction of the β phase ($V_{f,\beta}$) dominates as compared to that of the C15 phase in the TZFC alloys (Fig. 1). Table 1 summarizes the values of $V_{f,C15}$ and $V_{f,\beta}$ for the investigated TZFC alloys. The rod/particle-like morphologies can be seen in Fig. 1a and b insets captured for TZ52 and TZ54 respectively, whereas the eutectic morphologies can be in Fig. 1c and d insets for TZ72 and TZ74 respectively. It is also clear from Fig. 1 and Table 1 that Laves phases precipitate in the form of rod/particle-like morphologies with low volume fraction and then, rod-like morphologies transform into eutectic morphologies as the volume fraction of Laves phase increases due to poor solubility of solute elements.

Table 1. The volume fraction of C15 ($V_{f, C15}$) and β ($V_{f, \beta}$) phases, engineering yield strength ($\sigma_{0.2, E}$), ultimate strength ($\sigma_{max, E}$) and plastic strain ($\varepsilon_{p, E}$) along with the average hardness values of the investigated Ti-33Zr-xFe-yCr alloys. Note that the values of $V_{f, C15}$, $V_{f, \beta}$, $\sigma_{0.2, E}$, $\sigma_{max, E}$ and $\varepsilon_{p, E}$ are taken from the Ref. [10].

Alloys	**Chemical compositions**	$V_{f, Laves}$ **(%)**	$V_{f, \beta}$ **(%)**	$\sigma_{0.2, E}$ **(MPa)**	$\sigma_{max, E}$ **(MPa)**	$\varepsilon_{p, E}$ **(%)**	H_{avg} **(GPa)**
TZ52	Ti-33Zr-5Fe-2Cr	0.8	99.2	1128 ± 13	1830 ± 56	24.8 ± 2.5	3.50 ± 0.16
TZ54	Ti-33Zr-5Fe-4Cr	1.5	98.5	1210 ± 10	1711 ± 34	22.0 ± 0.5	3.69 ± 0.26
TZ72	Ti-33Zr-7Fe-2Cr	4.0	96.0	1239 ± 27	1901 ± 39	24.2 ± 2.6	3.94 ± 0.24
TZ74	Ti-33Zr-7Fe-2Cr	7.6	92.4	1285 ± 42	1566 ± 49	8.7 ± 1.2	4.08 ± 0.18

Table 1 also summarizes the engineering (compressive) mechanical properties of the investigated TZFC alloys, which were investigated in our previous finding [10]. However, true mechanical properties are also important as true compressive mechanical properties are helpful to predict the tensile behavior of alloys [28]. Therefore, in the present work, true mechanical properties of the investigated TZFC alloys have been investigated. Fig. 2 shows the true compressive stress versus strain curves of the investigated TZFC alloys. Table 2 presents the true mechanical properties obtained from the true stress versus strain curves of the investigated TZFC alloys. It can be seen from Tables 1 and 2 that the values of true yield strength and ultimate strength are lower than those of the engineering values of the investigated TZFC alloys, whereas the values of true plastic strain are greater than the values of engineering plastic strain for the investigated Ti-33Zr-xFe-yCr alloys [28]. This phenomenon happens because the cross-sectional area of the sample in compression testing increases as deformation continues [29]. Nonetheless, the reverse phenomenon occurs in tensile testing where true stress remains greater than engineering stress and true strain remains lower than engineering strain as the cross-sectional area of the sample in tensile testing decreases [29].

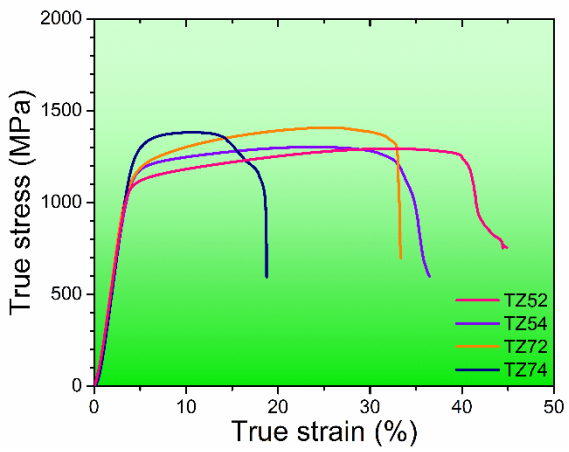

Fig. 2. The true compressive stress versus strain curves of the TZFC (Ti-33Zr-xFe-yCr) alloys. Note that the investigated TZFC (Ti-33Zr-xFe-yCr) alloys are labelled in the form of TZxy.

As the values of $V_{f,\,C15}$ increases the values of true yield strength increase, whereas the values of true compressive strain at failure and plastic strain decrease. Consequently, amongst the investigated TZFC alloys, TZ74 demonstrates the highest true yield strength (1223 ± 33 MPa), whereas TZ52 demonstrates the highest true compressive strain at failure (41.4 ± 2.4%) and plastic strain (37.0 ± 2.6%) as shown in Table 2. Fe and Cr possess low atomic radii than Ti, Fe and Cr in the investigated Ti-33Zr-xFe-yCr alloys, solid solution strengthening occurs, which is responsible to increase yield strength as the quantities of Fe and Cr increase in the TZFC alloys [17, 18]. Other than solid solution strengthening, precipitation strengthening also occurs in the investigated TZFC alloys due to the presence of C15 type Laves phase in the β matrix [10, 28, 30]. Furthermore, lamellar spacing present in the eutectic microstructure morphologies of Laves phase in TZ72 and TZ74 influences the mechanical properties of these alloys [10]. The measured values of lamellar spacing for TZ72 and TZ74 are 323 nm and 396 nm respectively. In general, the increase in lamellar spacing results in decreasing plastic strain and strength of an alloy [10]. Therefore, TZ72 displays large plastic strain and high strength as compared to TZ74.

Table 2. True yield strength ($\sigma_{0.2,\,T}$), ultimate strength ($\sigma_{max,\,T}$), compressive strain at failure ($\varepsilon_{f,\,T}$) and plastic strain ($\varepsilon_{p,\,T}$) of the investigated Ti-33Zr-xFe-yCr alloys.

Alloys	**Chemical compositions**	$\sigma_{0.2,\,T}$ **(MPa)**	$\sigma_{max,\,T}$ **(MPa)**	$\varepsilon_{f,\,T}$ **(%)**	$\varepsilon_{p,\,T}$ **(%)**
TZ52	Ti-33Zr-5Fe-2Cr	1083 ± 13	1304 ± 10	41.4 ± 2.4	37.0 ± 2.6
TZ54	Ti-33Zr-5Fe-4Cr	1135 ± 8	1290 ± 12	34.8 ± 1.3	30.4 ± 1.2
TZ72	Ti-33Zr-7Fe-2Cr	1171 ± 27	1402 ± 15	31.8 ± 1.9	27.2 ± 2.1
TZ74	Ti-33Zr-7Fe-2Cr	1223 ± 33	1337 ± 44	17.5 ± 1.0	13.1 ± 1.0

Fig. 3 shows the Vickers hardness values measured at three different loads for the investigated TZFC alloys and the corresponding average hardness values (of the three different loads) are presented in Table 1. It can be seen in Table 1 that hardness of the investigated TZFC alloys also increase as the quantities of Fe and Cr as well as the values of $V_{f,\,C15}$ increase. This indicates that yield strength and hardness in the present work increase because of the solid solution and precipitation strengthening effects [31]. In addition, Fig. 3 depicts that hardness values of the investigated TZFC alloys decrease as load in hardness testing increases from 3 kgf (HV3) to 30 kgf (HV30). This phenomenon occurs because of indentation size effects [21, 32]. Further, it can also be seen in Table 2 that as the content of Cr increases from 2 wt% in TZ52 and TZ72 to 4 wt% in TZ54 and TZ74, true ultimate strength declines, whereas as the content of Fe increases from 5 wt% in TZ52 and TZ54 to 7 wt% in TZ72 and TZ74, true ultimate strength increases. This indicates that Fe produces a better strengthening than Cr in the TZFC alloys. Based on the mechanical properties discussed in this work, it can be inferred that Ti-33Zr-5Fe-2Cr demonstrates the better combination of strength, plasticity and hardness as compared to other investigated alloys.

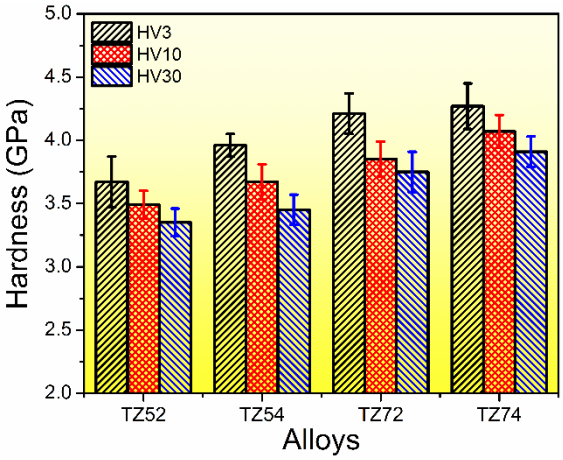

Fig. 3. Vickers hardness measured at 3 kgf (HV3), 10kgf (HV10) and 30 kgf (HV30) for the investigated Ti-33Zr-xFe-yCr alloys. Note that the investigated TZFC (Ti-33Zr-xFe-yCr) alloys are labelled in the form of TZxy.

Fig. 4 presents the size of the deformation zone around the indents taken at three different loads. Multiple measurements were taken to obtain the average values of the deformation zone size for the investigated TZFC alloys. It can be seen in Fig. 4 that the size of the deformation zone for all the TZFC alloys increases as the indentation load increases. However, among the investigated TZFC alloys, the size of the deformation zone decreases as the values of $V_{f,\,C15}$ increase. Therefore, the size of the deformation zone is inversely related to yield strength and hardness and directly related to compressive strain at failure and plastic strain for the TZFC alloys.

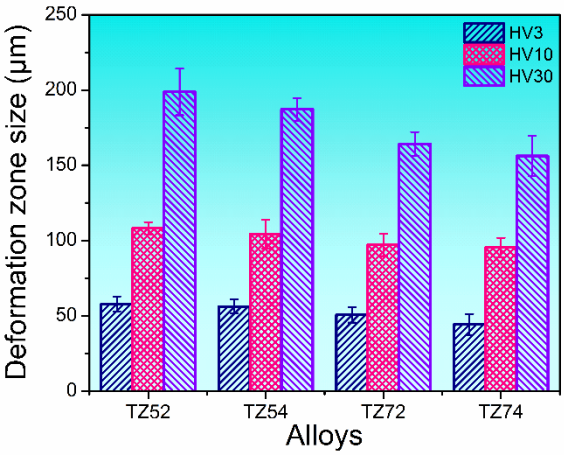

Fig. 4. The size of the deformation zone around the indents taken at 3 kgf (HV3), 10kgf (HV10) and 30 kgf (HV30) for the investigated Ti-33Zr-xFe-yCr alloys. Note that the investigated TZFC (Ti-33Zr-xFe-yCr) alloys are labelled in the form of TZxy.

Fig. 5 illustrates the optical micrographs of the Vickers indents taken at 30 kgf (HV30) for the investigated TZFC alloys. TZ52 and TZ54 display a greater number of slip bands as compared to TZ72 and TZ74 because TZ52 and TZ54 comprise lower values of $V_{f,\,C15}$ than TZ72 and TZ74 (Table 1). In fact, the cracks are found around the indentation-vertices of TZ72 and TZ74, whereas the cracks are not found around the indentation-vertices of TZ52 and TZ54. As TZ74 comprises the highest value of $V_{f,\,C15}$, two cracks are found around the indentation-vertices of TZ74. In general, solute particles produce lattice defect, whereas second phase possesses the different lattice configuration (crystal structure) [33, 34]. Consequently, solute particles and second phase morphologies impede the dislocations slip activities, which usually occur along the slip planes [33, 34]. Hence, TZ52 displays the highest number of slip bands and TZ74 displays the lowest number of slip bands around the micro-hardness indents among the investigated TZFC alloys (Fig. 5).

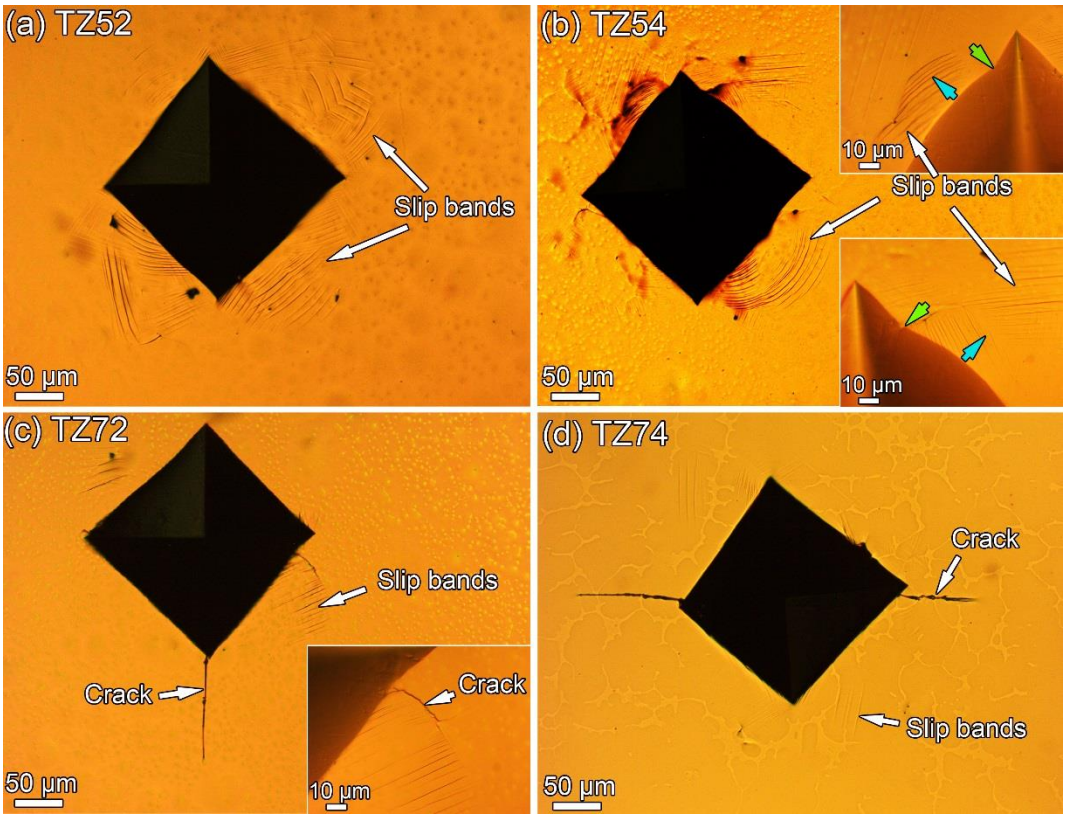

Fig. 5. Optical micrographs of the Vickers micro-indents taken at 30 kgf (HV30) for the investigated Ti-33Zr-xFe-yCr alloys. Note that the investigated TZFC (Ti-33Zr-xFe-yCr) alloys are labelled in the form of TZxy.

When an indenter penetrates the surface of a material, the underlying matter either flows away (pile-up) from the indenter-tip or flows down (sink-in) towards the indenter-tip [35]. Pile-up and sink-in phenomena affect the true contact area of indentation-impression and therefore, the actual area of indentation-impression remains different than the true contact area [35]. This tendency should be taken into consideration when estimating mechanical properties based on the area of indentation-impression. The pile-up and sink-in phenomena depend on the type of the indenter, underlying microstructure and dislocation motion that occurs in a specific grain [36, 37]. Pile-up usually happens in matrices with high plastic deformability and sink-in usually happens in matrices with low plastic deformability [35]. However, in case of multi-phase alloys, as dislocation activities remain different in each phase depending on the crystal structures of different phases, pile-up and sink-in phenomena take place differently over individual phases depending on the location of indentation. In the present work, pile-up occurs in some portions of the indentation-edges which are over β phase, whereas sink-in occurs in some portions of the indentation-edges which are over the Laves C15 phase. Small sky-blue and green colored arrows are used to show pile-up and sink-in respectively at indentation-edges in Fig. 5b for TZ54 as an example. Pile-up and sink-in morphologies indicate that dislocation activities in β phase should have occurred more than those in Laves C15 phase.

There are two types of cracks that usually form around indentation: Palmqvist and radial/median. The geometries of Palmqvist and radial/median cracks are shown in Fig. 6 [38]. Fracture toughness of brittle crystalline and amorphous materials can be estimated from the length of the cracks based on several models suggested by researchers depending on the type of crack formed [24, 25]. A specific type of crack around the indentation can be recognized based on its c/a value, where c is crack-length measured from indenter-tip and a is half of the diagonal length of indenter. The value of c/a remains < 2.5 for Palmqvist cracks, whereas c/a remains ≥ 2.5 for radial/median cracks [24, 25]. In the present work, the cracks are found

around the indents of TZ72 and TZ74. The values of *c*/*a* for TZ72 and TZ74 are 2.19 and 2.68 respectively. This indicates that the type of crack is Palmqvist in TZ72 and is radial/median in TZ74.

The various models, suitable for Palmqvist cracks, suggested by Shetty et al. [38, 39], Laugier [40], Casellas [41], Niihara et al. [39] and Lankford [39], have been used to estimate the indentation-based fracture toughness of TZ72 in this work. On the other hand, the various models, suitable for radial/median cracks, suggested by Anstis [41, 42], Evans & Charles [43], Tanaka [43], Laugier [44], Niihara et al. [45] and Lankford [39] have been used to estimate the indentation-based fracture toughness of TZ74 in this work. The corresponding equations of above-mentioned models are presented in Table 3.

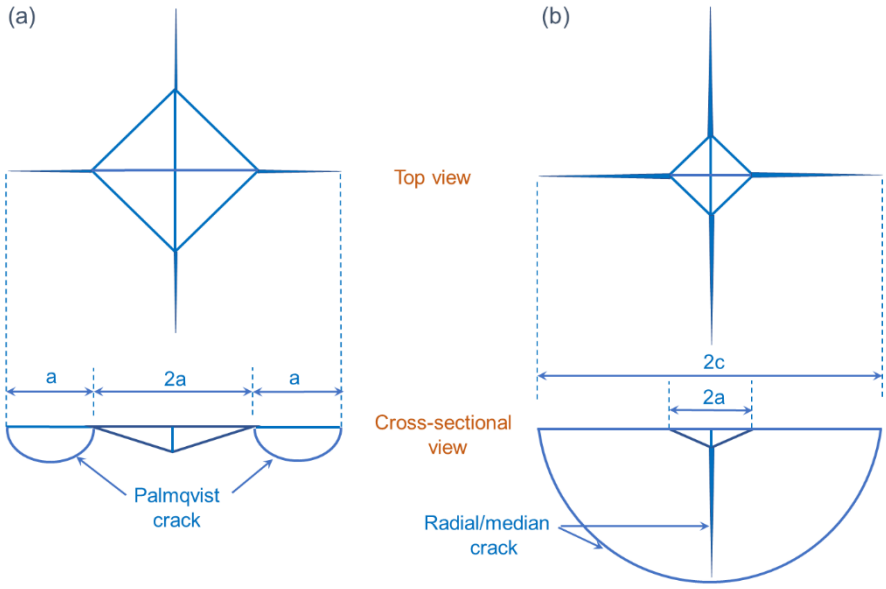

Fig. 6. The geometries of (a) Palmqvist and (b) radial/median cracks [38].

Table 3. Various models related to the Palmqvist and radial/median cracks to estimate the indentation-based fracture toughness. F is indentation load, a is half of the diagonal length of indenter, l is total length of crack/s measured from indentation vertices, c is crack-length measured from indenter-tip, E is elastic modulus (in GPa), H is Vickers hardness (in GPa).

Type of Crack	Models	Equations	Ref.

Palmqvist	Shetty et al.	$K_{Ic} = 0.0319 \cdot \left(\frac{F}{a \cdot l^{0.5}}\right)$	[39]
Palmqvist	Laugier	$K_{Ic} = 0.015 \cdot \left(\frac{F}{c^{1.5}}\right) \cdot \left(\frac{E}{H}\right)^{0.67} \cdot \left(\frac{l}{a}\right)^{-0.5}$	[40]
Palmqvist	Casellas	$K_{Ic} = 0.024 \cdot \left(\frac{F}{c^{1.5}}\right) \cdot \left(\frac{E}{H}\right)^{0.5}$	[41]
Palmqvist	Niihara et al.	$K_{Ic} = 0.0089 \cdot \left(\frac{E}{H}\right)^{0.4} \cdot \left(\frac{F}{a \cdot l^{0.5}}\right)$ for $0.25 < l/a < 2.5$	[39]
Palmqvist and Radial/Median	Lankford	$K_{Ic} = 0.0782 \cdot (H \cdot a^{0.5}) \cdot \left(\frac{E}{H}\right)^{0.4} \cdot \left(\frac{c}{a}\right)^{-1.56}$	[39]
Radial/Median	Anstis	$K_{Ic} = 0.016 \cdot \left(\frac{F}{c^{1.5}}\right) \cdot \left(\frac{E}{H}\right)^{0.5}$	[41, 42]
Radial/Median	Evans & Charles	$K_{Ic} = 0.0752 \cdot \left(\frac{F}{c^{1.5}}\right)$	[43]
Radial/Median	Tanaka	$K_{Ic} = 0.0725 \cdot \left(\frac{F}{c^{1.5}}\right)$	[43]
Radial/Median	Laugier	$K_{Ic} = 0.022 \cdot \left(\frac{E}{H}\right)^{0.4} \cdot \left(\frac{F}{c^{1.5}}\right)$	[44]
Radial/Median	Niihara et al.	$K_{Ic} = 0.0309 \cdot \left(\frac{E}{H}\right)^{0.4} \cdot \left(\frac{F}{c^{1.5}}\right)$	[45]

Fig. 7 shows the fracture toughness of TZ72 and TZ74. Lankford model suggested in Table 3 can be used for both the kinds of cracks, i.e., Palmqvist and radial/median. Niihara et al. [39, 45] and Laugier [40, 44] have suggested different models for each type of crack (Table 3). Among the various model used in this work, Lankford model estimates the lowest value of fracture toughness for TZ72 (4.43 MPa $m^{1/2}$) and TZ74 (3.19 MPa $m^{1/2}$). Further, the Laugier model estimates the highest value of fracture toughness (10.76 MPa $m^{1/2}$) among the models used for TZ72, whereas the model suggested by Niihara et al. [45] estimates the highest value of fracture toughness (6.58 MPa $m^{1/2}$) among the models used for TZ74. It is clear from Fig. 7 that, TZ72 exhibits the higher fracture toughness values than TZ74. This also indicates that the fracture toughness of an alloy (TZ74) comprising radial/median crack/s remains lower than that of an alloy (TZ72) comprising Palmqvist crack/s. It can be deduced based on the results

shown in Fig. 7 that fracture toughness of an alloy directly correlates to the volume fraction of Laves phase of an alloy.

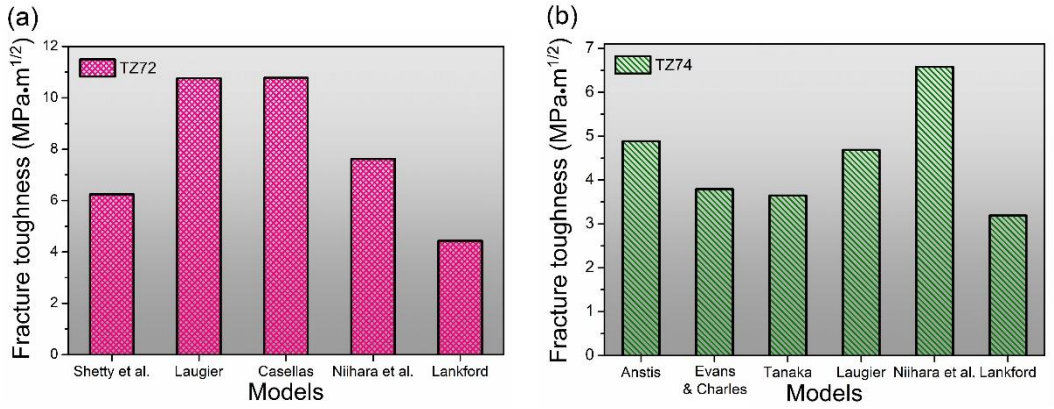

Fig. 7. Vickers indentation-based fracture toughness measured based on the various models for (a) TZ72 (Ti-33Zr-7Fe-2Cr) and (b) TZ74 (Ti-33Zr-7Fe-4Cr).

4. Conclusions

The microstructures, the true mechanical properties, the deformation and crack features around the hardness indents of the Ti-33Zr-xFe-yCr (x = 5, 7 wt% and y = 2, 4 wt%) alloys have been evaluated along with the indentation-based fracture toughness of Ti-33Zr-7Fe-2Cr and Ti-33Zr-7Fe-4Cr. The followings are the concluding remarks of the present work.

- The volume fraction of C15 phase increases as the quantities of Fe and Cr in the Ti-33Zr-xFe-yCr alloys increase.
- Among the investigated Ti-33Zr-xFe-yCr alloys, Ti-33Zr-7Fe-4Cr demonstrates the highest true yield strength (1223 ± 33 MPa) and hardness (4.08 ± 0.18 GPa), whereas Ti-33Zr-5Fe-2Cr shows the highest true compressive strain at failure (41.4 ± 2.4%) and true plastic strain (37.0 ± 2.6%).
- The variation in the volume fraction of C15 type Laves phase is effective in tailoring the mechanical properties of the investigated Ti-33Zr-xFe-yCr alloys.

- The size of deformation zone relates inversely with the volume fraction of the C15 type Laves phase, which reveals the superior strengthening ability of the C15 type Laves phase.
- Palmqvist crack is found in Ti-33Zr-7Fe-2Cr, whereas radial/median crack is found in Ti-33Zr-7Fe-4Cr. Hence, Ti-33Zr-7Fe-2Cr displays a better fracture toughness than Ti-33Zr-7Fe-2Cr.
- Among the investigated Ti-33Zr-xFe-yCr alloys, Ti-33Zr-5Fe-2Cr comprises a better combination of strength, plasticity and hardness.

References

[1] C.D. Rabadia, Y.J. Liu, S.F. Jawed, L. Wang, Y.H. Li, X.H. Zhang, T.B. Sercombe, H. Sun, L.C. Zhang, Improved deformation behavior in Ti-Zr-Fe-Mn alloys comprising the C14 type Laves and β phases, Mater. Des. 160 (2018) 1059-1070. https://doi.org/10.1016/j.matdes.2018.10.049.

[2] A.V. Kazantzis, M. Aindow, I.P. Jones, G.K. Triantafyllidis, J.T.M. De Hosson, The mechanical properties and the deformation microstructures of the C15 Laves phase Cr_2Nb at high temperatures, Acta Mater. 55 (2007) 1873-1884. https://doi.org/10.1016/j.actamat.2006.10.048.

[3] J. Nei, K. Young, S.O. Salley, K.Y.S. Ng, Determination of C14/C15 phase abundance in Laves phase alloys, Mater. Chem. Phys. 136 (2012) 520-527. https://doi.org/10.1016/j.matchemphys.2012.07.020.

[4] S. Banerjee, A. Kumar, P. Ruz, P. Sengupta, Influence of Laves phase on microstructure and hydrogen storage properties of Ti–Cr–V based alloy, Int. J. Hydrogen Energy 41 (2016) 18130-18140. https://doi.org/10.1016/j.ijhydene.2016.07.088.

[5] F. Stein, M. Palm, G. Sauthoff, Structure and stability of Laves phases. Part I. Critical assessment of factors controlling Laves phase stability, Intermetallics 12 (2004) 713-720. https://doi.org/10.1016/j.intermet.2004.02.010.

[6] Y. Nakagawa, T. Ohta, Y. Kaneno, H. Inoue, T. Takasugi, Defect structures and room-temperature mechanical properties of C15 laves phases in Zr-Nb-Cr and Zr-Hf-Cr alloy systems, Metall. Mater. Trans. A 35 (2004) 3469-3476. https://doi.org/10.1007/s11661-004-0184-7.

[7] K.C. Chen, S.M. Allen, J.D. Livingston, Factors affecting the room-temperature mechanical properties of $TiCr_2$-base Laves phase alloys, Mater. Sci. Eng. A 242 (1998) 162-173. https://doi.org/10.1016/S0921-5093(97)00526-1.

[8] K.C. Chen, F. Chu, P.G. Kotula, D. Thoma, $HfCo_2$ Laves phase intermetallics—part II: elastic and mechanical properties as a function of composition, Intermetallics 9 (2001) 785-798. https://doi.org/10.1016/S0966-9795(01)00067-X.

[9] A.J. Knowles, A. Bhowmik, S. Purkayastha, N.G. Jones, F. Giuliani, W.J. Clegg, D. Dye, H.J. Stone, Laves phase intermetallic matrix composite in situ toughened by ductile precipitates, Scr. Mater. 140 (2017) 59-62. https://doi.org/10.1016/j.scriptamat.2017.06.043.

[10] C.D. Rabadia, Y.J. Liu, L. Wang, H. Sun, L.C. Zhang, Laves phase precipitation in Ti-Zr-Fe-Cr alloys with high strength and large plasticity, Mater. Des. 154 (2018) 228-238. https://doi.org/10.1016/j.matdes.2018.05.035.

[11] L.-C. Zhang, L.-Y. Chen, L. Wang, Surface Modification of Titanium and Titanium Alloys: Technologies, Developments and Future Interests, Adv. Eng. Mater. 22 (2020) 1901258. https://doi.org/10.1002/adem.201901258.

[12] J.C. Wang, Y.J. Liu, P. Qin, S.X. Liang, T.B. Sercombe, L.C. Zhang, Selective laser melting of Ti–35Nb composite from elemental powder mixture: Microstructure, mechanical behavior and corrosion behavior, Mater. Sci. Eng. A 760 (2019) 214-224. https://doi.org/10.1016/j.msea.2019.06.001.

[13] L.C. Zhang, D. Klemm, J. Eckert, Y.L. Hao, T.B. Sercombe, Manufacture by selective laser melting and mechanical behavior of a biomedical Ti–24Nb–4Zr–8Sn alloy, Scr. Mater. 65 (2011) 21-24. https://doi.org/10.1016/j.scriptamat.2011.03.024.

[14] L.C. Zhang, L.Y. Chen, A Review on Biomedical Titanium Alloys: Recent Progress and Prospect, Adv. Eng. Mater. 21 (2019) 1801215. https://doi.org/10.1002/adem.201801215.

[15] L.C. Zhang, Y. Liu, S. Li, Y. Hao, Additive Manufacturing of Titanium Alloys by Electron Beam Melting: A Review, Adv. Eng. Mater. 20 (2018) 1700842. https://doi.org/10.1002/adem.201700842.

[16] S.F. Jawed, C.D. Rabadia, Y.J. Liu, L. Wang, Y.H. Li, X.H. Zhang, L.C. Zhang, Beta-type Ti-Nb-Zr-Cr alloys with large plasticity and significant strain hardening, Mater. Des. 181 (2019) 108064. https://doi.org/10.1016/j.matdes.2019.108064.

[17] C.D. Rabadia, Y.J. Liu, G.H. Cao, Y.H. Li, C.W. Zhang, T.B. Sercombe, H. Sun, L.C. Zhang, High-strength β stabilized Ti-Nb-Fe-Cr alloys with large plasticity, Mater. Sci. Eng. A 732 (2018) 368-377. https://doi.org/10.1016/j.msea.2018.07.031.

[18] S.F. Jawed, C.D. Rabadia, Y.J. Liu, L.Q. Wang, Y.H. Li, X.H. Zhang, L.C. Zhang, Mechanical characterization and deformation behavior of β-stabilized Ti-Nb-Sn-Cr alloys, J. Alloys Compd. 792 (2019) 684-693. https://doi.org/10.1016/j.jallcom.2019.04.079.

[19] L.C. Zhang, J. Das, H.B. Lu, C. Duhamel, M. Calin, J. Eckert, High strength Ti–Fe–Sn ultrafine composites with large plasticity, Scr. Mater. 57 (2007) 101-104. https://doi.org/10.1016/j.scriptamat.2007.03.031.

[20] L.-C. Zhang, H.-B. Lu, C. Mickel, J. Eckert, Ductile ultrafine-grained Ti-based alloys with high yield strength, Appl. Phys. Lett. 91 (2007) 051906. https://doi.org/10.1063/1.2766861.

[21] C.D. Rabadia, Y.J. Liu, L.Y. Chen, S.F. Jawed, L.Q. Wang, H. Sun, L.C. Zhang, Deformation and strength characteristics of Laves phases in titanium alloys, Mater. Des. 179 (2019) 107891. https://doi.org/10.1016/j.matdes.2019.107891.
[22] T. To, F. Célarié, C. Roux-Langlois, A. Bazin, Y. Gueguen, H. Orain, M. Le Fur, V. Burgaud, T. Rouxel, Fracture toughness, fracture energy and slow crack growth of glass as investigated by the Single-Edge Precracked Beam (SEPB) and Chevron-Notched Beam (CNB) methods, Acta Mater. 146 (2018) 1-11. https://doi.org/10.1016/j.actamat.2017.11.056.
[23] C. Zehnder, K. Czerwinski, K.D. Molodov, S. Sandlöbes-Haut, J.S.K.L. Gibson, S. Korte-Kerzel, Plastic deformation of single crystalline C14 Mg_2Ca Laves phase at room temperature, Mater. Sci. Eng. A 759 (2019) 754-761. https://doi.org/10.1016/j.msea.2019.05.092.
[24] D. Ćorić, M. Majić Renjo, L. Ćurković, Vickers indentation fracture toughness of Y-TZP dental ceramics, Int. J. Refract. Met. Hard Mater. 64 (2017) 14-19. https://doi.org/10.1016/j.ijrmhm.2016.12.016.
[25] S. Zameer Abbas, F. Ahmad Khalid, H. Zaigham, Indentation fracture toughness behavior of FeCo-based bulk metallic glass intrinsic composites, J. Non-Cryst. Solids 457 (2017) 86-92. https://doi.org/10.1016/j.jnoncrysol.2016.11.022.
[26] B. Song, B. Sanborn, Relationship of compressive stress-strain response of engineering materials obtained at constant engineering and true strain rates, Int. J. Impact Eng. 119 (2018) 40-44. https://doi.org/10.1016/j.ijimpeng.2018.05.001.
[27] D.J. Thoma, J.H. Perepezko, A geometric analysis of solubility ranges in Laves phases, J. Alloys Compd. 224 (1995) 330-341. https://doi.org/10.1016/0925-8388(95)01557-4.
[28] C.D. Rabadia, Y.J. Liu, C.H. Zhao, J.C. Wang, S.F. Jawed, L.Q. Wang, L.Y. Chen, H. Sun, L.C. Zhang, Improved trade-off between strength and plasticity in titanium based metastable beta type Ti-Zr-Fe-Sn alloys, Mater. Sci. Eng. A 766 (2019) 138340. https://doi.org/10.1016/j.msea.2019.138340.
[29] J. Chakrabarty, Applied plasticity, Springer, New York, 2000.
[30] Y. Wang, L. Yang, X.L. Shi, X. Shi, L. Chen, M.S. Dargusch, J. Zou, Z.G. Chen, Flexible thermoelectric materials and generators: challenges and innovations, Adv. Mater. 31 (2019) 1807916. https://doi.org/10.1002/adma.201807916.
[31] S.F. Jawed, C.D. Rabadia, Y.J. Liu, L.Q. Wang, P. Qin, Y.H. Li, X.H. Zhang, L.C. Zhang, Strengthening mechanism and corrosion resistance of beta-type Ti-Nb-Zr-Mn alloys, Mater. Sci. Eng. C 110 (2020) 110728. https://doi.org/10.1016/j.msec.2020.110728.
[32] B.D. Beake, A.J. Harris, J. Moghal, D.E.J. Armstrong, Temperature dependence of strain rate sensitivity, indentation size effects and pile-up in polycrystalline tungsten from 25 to 950 °C, Mater. Des. 156 (2018) 278-286. https://doi.org/10.1016/j.matdes.2018.06.063.
[33] A.P. Mouritz, Introduction to aerospace materials, Elsevier, Cambridge, 2012.
[34] D. Hull, D.J. Bacon, Introduction to Dislocations, fifth ed., Butterworth-Heinemann, Oxford, 2011.
[35] A.E. Giannakopoulos, S. Suresh, Determination of elastoplastic properties by instrumented sharp indentation, Scr. Mater. 40 (1999) 1191-1198. https://doi.org/10.1016/S1359-6462(99)00011-1.
[36] M.Y. N'jock, D. Chicot, J.M. Ndjaka, J. Lesage, X. Decoopman, F. Roudet, A. Mejias, A criterion to identify sinking-in and piling-up in indentation of materials, Int. J. Mech. Sci. 90 (2015) 145-150. https://doi.org/10.1016/j.ijmecsci.2014.11.008.
[37] G. Muthupandi, K.R. Lim, Y.-S. Na, J. Park, D. Lee, H. Kim, S. Park, Y.S. Choi, Pile-up and sink-in nanoindentation behaviors in AlCoCrFeNi multi-phase high entropy alloy, Mater. Sci. Eng. A 696 (2017) 146-154. https://doi.org/10.1016/j.msea.2017.04.045.
[38] D.K. Shetty, I.G. Wright, P.N. Mincer, A.H. Clauer, Indentation fracture of WC-Co cermets, J. Mater. Sci. 20 (1985) 1873-1882. https://doi.org/10.1007/bf00555296.
[39] A. Şakar‐Deliormanli, M. Güden, Microhardness and fracture toughness of dental materials by indentation method, J. Biomed. Mater. Res. B Appl. Biomater. 76 (2006) 257-264. https://doi.org/10.1002/jbm.b.30371.
[40] M.T. Laugier, New formula for indentation toughness in ceramics, J. Mater. Sci. Lett. 6 (1987) 355-356. https://doi.org/10.1007/bf01729352.
[41] M.C.C.d.S. Moraes, C.N. Elias, J. Duailibi Filho, L.G.d. Oliveira, Mechanical properties of alumina-zirconia composites for ceramic abutments, Mater. Res. 7 (2004) 643-649. https://doi.org/10.1590/S1516-14392004000400021
[42] G. Anstis, P. Chantikul, B.R. Lawn, D. Marshall, A critical evaluation of indentation techniques for measuring fracture toughness: I, direct crack measurements, J. Am. Ceram. Soc. 64 (1981) 533-538. https://doi.org/10.1111/j.1151-2916.1981.tb10320.x.
[43] A. Nastic, A. Merati, M. Bielawski, M. Bolduc, O. Fakolujo, M. Nganbe, Instrumented and Vickers Indentation for the Characterization of Stiffness, Hardness and Toughness of Zirconia Toughened Al2O3 and SiC Armor, J. Mater. Sci. Technol. 31 (2015) 773-783. https://doi.org/10.1016/j.jmst.2015.06.005.

[44] M.T. Laugier, The elastic/plastic indentation of ceramics, J. Mater. Sci. Lett. 4 (1985) 1539-1541. https://doi.org/10.1007/bf00721390.
[45] K. Niihara, R. Morena, D.P.H. Hasselman, Evaluation of K_{Ic} of brittle solids by the indentation method with low crack-to-indent ratios, J. Mater. Sci. Lett. 1 (1982) 13-16. https://doi.org/10.1007/bf00724706.